CrossMark

Vortex-induced vibration dynamics of a flexible fluid-conveying marine riser subjected to axial harmonic tension

Xiaodong Zhang[1] · Ruyi Gou[1] · Wenwu Yang[1] · Xueping Chang[1]

Abstract

This study investigates vortex-induced vibration dynamic responses of a marine riser transporting internal flow under the action of axial harmonic tension by means of finite element method. A van der Pol wake oscillator is adopted to represent the fluctuating lift forces, and nonlinear hydrodynamic force is also introduced. The goal of the present work is to discuss VIV dynamic responses of a fluid-conveying riser to guide the design and usage of riser in offshore oil field. The constant tension analyses are first obtained to determine the lock-in region of cross-flow velocity. Then, the influence of excitation frequency and harmonic tension amplitude on the resonance regions, the displacement amplitudes, the maximum stresses for various internal flow velocity, has been investigated. The results show that the dominated resonance region changed from twice the fundamental frequency to the fundamental frequency when harmonic tension amplitudes and cross-flow velocities are simultaneously increased. It is also revealed that the foremost two lock-in regions, respectively, appeared near the fundamental frequency and twice the fundamental frequency for varying cross-flow velocities.

Abbreviations

x, y, z	Coordinate directions (m)
w	Cross-flow displacement (m)
L	Length of riser (m)
D	Outer diameter (m)
D_i	Inner diameter (m)
ρ_p	Pipe density (kg/m^3)
ρ_o	Outer fluid density (kg/m^3)
ρ_i	Internal fluid density (kg/m^3)
C_a	Added mass coefficient [$C_a = m_d/(\rho_o \pi D^2/4)$]
m_p	Pipe mass per unit length (kg/m)
m_f	Internal fluid mass per unit length (kg/m)
m_d	Additional fluid mass per unit length (kg/m)
U_o	Cross-flow velocity (m/s)
U_i	Internal fluid velocity (m/s)
v	Non-dimensional internal fluid velocity ($v = LU_i\sqrt{m_f/(EI)}$)
E	Elasticity modulus (Pa)
c	Damping coefficient (N/s)
ζ	Non-dimensional damping coefficient [$\zeta = c/(2m\omega_1)$]
I	Moment of inertia (m^4)
A_o	Section area of pipe (m^2)
T_t	Top pre-tension (N)
T	Static effective tension, N
T_0	Constant tension (N)
T_1	Harmonic tension (N)
k	Constant tension coefficient [$k = T_0/((m_p + m_f - m_d)gL)$]
a	Harmonic tension coefficient ($a = T_0/T_1$)
ω	Harmonic tension circular frequency (rad/s)
g	Gravitational acceleration (m/s^2)
F_f	Cross-flow hydrodynamic force (N)

✉ Ruyi Gou
  2009swpu@163.com

[1] School of Mechatronic Engineering, Southwest Petroleum University, Chengdu 610500, China

1 Introduction

In ocean engineering, marine risers are widely used to well drilling and production of oil and gas resources. Their performance directly affects the production efficiency,

economy, and reliability of field exploration and development. However, the marine riser is inevitably subjected to the surrounding environmental loads, such as waves and currents. Furthermore, vortex-induced vibrations (VIVs) of a flexible marine riser immersed in currents have a significant effect on the fatigue damage and lifetime [1–3]. In order to suppress the VIV responses of the riser under external forces, some mechanisms induced by combination of both VIV and other excitations need to be investigated in detail.

The methods studying VIV mainly include experiments, computational fluid dynamics (CFDs) and analytical models for both elastically supported rigid cylinders and long flexible cylinders in the last decades [4–7]. Some literature reviews have been discussed in detail [8–12].

As for rigid cylinders, one of the difficulties is how to enhance the accuracy of analytical model. A refined wake oscillator described the cross-flow (CF) motion of an elastically supported rigid cylinder was first proposed [13]. Next, the importance effects of geometric and hydrodynamic nonlinearities on the accuracy of response amplitudes for combination of both CF and in-line (IL) motions of rigid cylinder were examined and verified [14, 15]. Furthermore, an modified hydrodynamic force was proposed and examined [16].

Concerning the developments of VIV models of slender cylinders, most studies mainly focus on the CF and IL vibration of the riser. An analysis model to predict the CF VIV response for variable-tension vertical risers under linear shear flow was developed [17]. Some external excitations, such as internal fluids, pulsating internal flow and base excitations, were investigated for the CF VIV dynamics of fluid-conveying risers [18–20]. Recently, a nonlinear hydrodynamic force that described CF VIV dynamics of a fluid-conveying pipe with a CF excitation under uniform currents was proposed and analyzed [21]. A literature that focused on the CF VIV of a flexible pipe transporting an internal fluid from subcritical to supercritical subjected to the CF and axial (AX) motions was presented [22]. An improved time domain coupled model of CF and IL VIV for flexible risers was also proposed [23]. Although some simplified geometry nonlinearities were included in these models, these prediction models pay little attention on the effect of nonlinear hydrodynamic force for VIV of a flexible riser.

In order to fully improve the vibration model of a flexible riser, some researchers dedicated themselves to develop a three-dimensional (3D) VIV prediction model. A 3D VIV prediction model of a flexible pipe with geometric nonlinearity had been firstly established and investigated [24, 25]. Then, 3D VIV model of a long flexible pipe within geometric and hydrodynamic nonlinearities immersed in uniform flow was performed by using finite

difference method (FDM) [26], and the results agreed well with experimental data [27]. The nonlinear 3D VIV dynamic responses of a marine viscoelastic riser subjected to uniform flow were also discussed [28]. Yang et al. [29] presented a 3D VIV model for a fluid-conveying pipe. It has to emphasize that the top tension excitation effect of a flexible riser was neglected in these studies. But the top tension excitation phenomenon widely occurs in marine risers.

Recently, the effects of pre-tension and axial stiffness on vibration amplitudes and suppression characteristics were experimentally investigated [30]. Then, experiments and numerical simulations were performed to investigate dynamic responses of a flexible riser subjected to top axial harmonic excitation in detail [31–33]. Although these researches explore some excitation mechanisms, it should be emphasized that the hydrodynamic force in their model is elaborated by the Morison's expression rather than wake vortex oscillator model. Furthermore, the conveying internal fluid in a pipe is neglected in aforementioned models.

In this paper, a CF VIV model of a flexible riser transporting internal flows, including axial harmonic tension, is proposed for the first time. It should be noted that the tension varies on both space and time. Moreover, the nonlinear hydrodynamic force is introduced in this study. The verification of the model and method is discussed in detail. The effects of constant tension, harmonic tension amplitude and frequency on the displacement amplitudes, the maximum CF bending stresses, lock-in regions and frequency responses are investigated.

2 Mathematical models

2.1 Equation of motion of a fluid-conveying pipe

In this paper, a pipe transporting internal fluid which is perfectly straight at its vertical static equilibrium under the effective weight is fully immersed in water. The flexible riser simply supported at both ends is placed in uniform currents aligned with z direction, as depicted in Fig. 1.

Following the literatures [26] and [21], the partial differential equation of CF motion of a flexible fluid-conveying riser is obtained:

$$m\ddot{w} + c\dot{w} + EIw^{(IV)} + 2m_f U_i \dot{w}'$$
$$+ \left(m_f U_i^2 - \frac{EA_o}{2L} \int_0^L w'^2 dx \right) w'' - (Tw')'$$
$$= F_f(z, t) \tag{1}$$

where w represents the transverse displacements of the pipe, $m = m_p + m_f + m_d$ where m_p, m_f and m_d are the mass
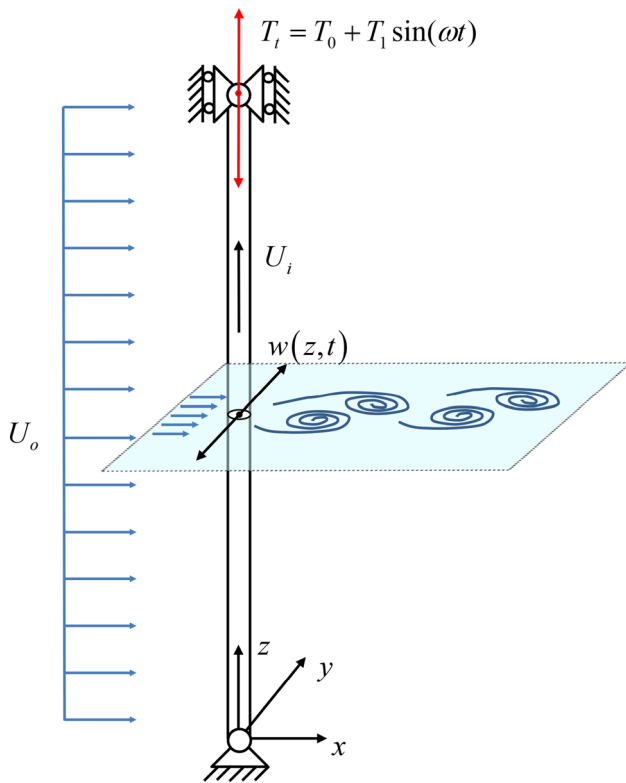
Fig. 1 A schematic model of the flexible riser subjected to VIV

per unit length of the flexible pipe, the internal fluid and additional fluid mass where ρ_o in $m_d = C_a \rho_o \pi D^2 / 4$ (the added mass coefficient $C_a = 1$ for cylinder) is the CF density, respectively. The $F_f(z, t)$ denotes the hydrodynamic force which is acted on the flexible pipe. The structural parameters of the pipe include length (L), outer diameter (D), internal diameter (D_i) and moment of inertia (I), and the material parameters are a constant Yong's modulus (E) and damping coefficient (c) defined by $2m\omega_1\zeta$ in which ω_1 is the fundamental frequency of the riser and ζ is non-dimensional damping coefficient.

The static effective tension T can be spatially varied along z coordinate considering the gravity and bouncy effects, namely $T = T_t - (m_p + m_f - m_d)g(L - z)$, where T_t is the top pre-tension and g is the gravity. The top pre-tension $T_t = T_0 + T_1 \sin(\omega t)$ is introduced to characterize the axial harmonic tension in which the top constant pre-tension $T_0 = k(m_p + m_f - m_d)gL$ is k times the resultant force of gravity and buoyancy and harmonic tension amplitude $T_1 = aT_0$ is a times the constant pre-tension T_0. The k and a are named constant tension coefficient and harmonic tension coefficient, respectively. The ω is the top harmonic tension circular frequency.

The simply supported boundary conditions of the marine riser are expressed as follows:

$$w(0, t) = 0, \quad w''(0, t) = 0, \quad w(L, t) = 0, \quad w''(L, t) = 0 \tag{2}$$

2.2 Nonlinear hydrodynamic force model

The CF hydrodynamic force acting on the riser, $F_f(z, t)$, can be determined as a cross-flow projection of the total hydrodynamic force on the y direction, which includes the sectional vortex-induced drag force $\vec{F}_D$ and lift fore $\vec{F}_L$, as illustrated in Fig. 2. The drag and lift forces identify with IL and CF directions, respectively. Therefore, the drag force and lift force can be obtained:

$$\vec{F}_D = \frac{1}{2} C_D \rho_o D |\vec{U}_{oR}| \left(U_o \vec{i} - \frac{\partial w}{\partial t} \vec{j} \right) \tag{3}$$

$$\vec{F}_L = \frac{1}{2} C_L \rho_o D |\vec{U}_{oR}| \left(\frac{\partial w}{\partial t} \vec{i} + U_o \vec{j} \right) \tag{4}$$

in which C_D and C_L denote mean drag coefficients and time-varying lift coefficients, respectively. The relative velocity $\vec{U}_{oR}$ between cross-flow and riser can be expressed as

$$\vec{U}_{oR} = \left(U_o - \frac{\partial x}{\partial t} \right) \vec{i} - \frac{\partial w}{\partial t} \vec{j} \tag{5}$$

Following the references [16] and [21], considering the relative velocities of the cross-flow around the riser IL motion ($U_o - \dot{w}$) and neglecting the smaller CF velocity, the projected CF hydrodynamic forces can be described as follows:
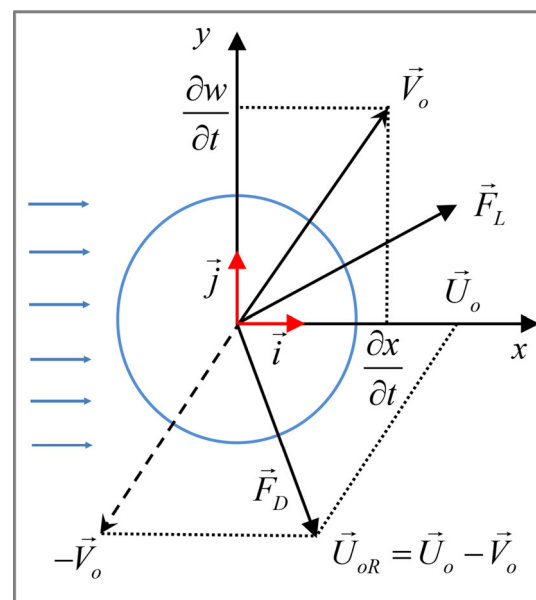

Fig. 2 Drag force $\vec{F}_D$ along with relative flow velocity $\vec{U}_{oR}$ and lift force $\vec{F}_L$ in perpendicular direction

$$F_{\mathrm{f}}(z,t) = (\vec{F}_{\mathrm{L}} + \vec{F}_{\mathrm{D}}) \cdot \vec{j} = \frac{1}{2} C_{\mathrm{L}} \rho_{\mathrm{o}} D U_{\mathrm{o}} \left[1 + \frac{1}{2U_{\mathrm{o}}^2} \left(\frac{\partial w}{\partial t} \right)^2 \right] U_{\mathrm{o}}$$
$$- \frac{1}{2} C_{\mathrm{D}} \rho_{\mathrm{o}} D U_{\mathrm{o}} \left[1 + \frac{1}{2U_{\mathrm{o}}^2} \left(\frac{\partial w}{\partial t} \right)^2 \right] \frac{\partial w}{\partial t} \tag{6}$$

The wake variable $q(z,t) = 2C_{\mathrm{L}}/C_{\mathrm{L0}}$ [13] is introduced to represent the time-varying lift coefficients, and the variations of q are obtained:

$$\ddot{q} + \lambda w_{\mathrm{s}} (q^2 - 1) \dot{q} + w_{\mathrm{s}}^2 q = \frac{P}{D} \ddot{w} \tag{7}$$

where $w_{\mathrm{s}} = 2\pi St U_{\mathrm{o}}/D$ denotes the vortex-shedding circular frequency, the right hand side of equation denotes excitation term characterizing the influence of riser motion on the near wake related to the acceleration of riser, λ is van der Pol parameter, P denotes the coupling empirical coefficients. In this article, the values of empirical parameters are $C_D = 1.2$, $C_{\mathrm{L0}} = 0.3$, $P = 12$, $\lambda = 0.3$ and $St = 0.2$. Furthermore, the non-dimensional internal fluid velocity is expressed as $v = \mathrm{L}U_{\mathrm{i}}\sqrt{m_{\mathrm{f}}/(\mathrm{EI})}$.

3 Comparisons of numerical methods

To verify the results of numerical simulations, the model parameters of a flexible pipe with $L = 15$ m were adopted to compare with the results of Ref. [21] under uniform currents, and it is noted that their model only includes gravity and buoyancy without considering top tension. Analysis parameters of a flexible pipe related to numerical investigations are formulated in Table 1. The coupled nonlinear partial-differential equations are implemented in COMSOL program by FEM. Initial conditions are assigned in the initial state for the flexible riser ($w = \dot{w} = 0$), with

Table 1 Physical parameters used for numerical study

Parameter	Description	Value
E	Yong's modulus (GN/m^2)	210
L	Length (m)	150
D	Outer diameter (m)	0.25
D_{i}	Inner diameter (m)	0.125
ρ_{p}	Pipe density (kg/m^3)	7800
ρ_{o}	Outer fluid density (kg/m^3)	1020
ρ_{f}	Inner fluid density (kg/m^3)	870
U_{o}	Cross-flow velocity (m/s)	0–0.35
v	Internal fluid velocity (1)	0–2
k	Top tension coefficient (1)	1–3
ζ	Damping ratio (1)	0.005

$q = 2$ ($\dot{q} = 0$) for wake variables. The flexible pipe is dispersed in 1500 elements which satisfies the error 10e−5; the time step is 0.005 s.

The hydrodynamic force on the hand right side of Eq. (1) is removed to evaluate the foremost two natural frequencies for various non-dimensional internal velocities; the results of frequency analyses are formulated in Table 2. It is observed from Table 2 that the results of modal analysis by FEM agree well with those data in the literature [21]. The CF displacement amplitudes validated the VIV prediction by the literature [18] are plotted in Fig. 3. Inspecting the plotted curves in Fig. 3, it is noted that the results of the two analytical methods are in good agreement. Therefore, it can be revealed that the FEM can effectively and accurately calculate the coupled model.

4 Parametric investigations and discussions

In this section, the impact of top constant pre-tension on natural frequencies, displacements and stresses is first investigated to determine the lock-in regions. Then, three kinds of internal fluid velocity located in pre-synchronization, synchronization and post-synchronization are investigated. In the following analysis, the non-dimensional internal fluid velocity is unity, the tension coefficient $k = 2$ and the length of riser $L = 150$ m is selected in subsection 4.

4.1 The effect of internal flow under constant pre-tension

The effects of internal flow on the fundamental frequencies and displacement amplitudes are, respectively, depicted in Figs. 4 and 5 under constant pre-tension. It can be seen from Fig. 4 that an increase in tension coefficient results in the increase in fundamental frequency for all of non-dimensional internal fluid velocities. The natural frequencies first increase rapidly and then increase slowly with an increase in tension coefficient for various internal fluid velocities. Inspecting Figs. 4 and 5, it is revealed that the internal fluid velocity has little impact on fundamental frequency and displacement amplitude.

4.2 The effect of top constant pre-tension

Based on aforementioned analyses, model analyses are carried out to analyze the impact of tension coefficient on the first two natural frequencies of the fluid-conveying pipe when $v = 1$, as listed in Table 3.

The influences of tension coefficient on displacement amplitudes are portrayed in Fig. 6. It is found from Fig. 6

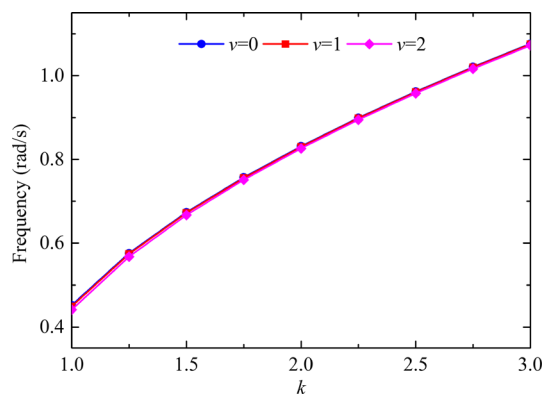**Table 2** Comparisons of natural frequencies in still water when $L = 15$ m

Non-dimensional internal fluid velocity (v)	Internal fluid velocity U_i (m/s)	First natural frequency (rad/s)		Second natural frequency (rad/s)	
		He et al. [21]	FEM	He et al. [21]	FEM
0	0	14.35	14.35	57.70	57.70
1	125.36	13.59	13.59	56.98	56.97
2	250.72	11.00	11.00	54.76	54.71
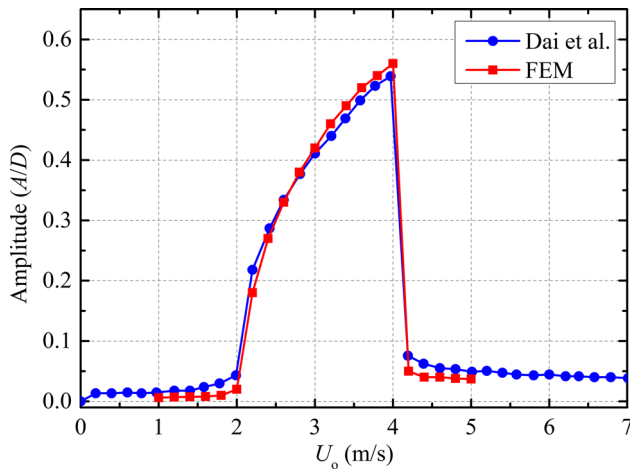
Fig. 3 Displacement amplitudes of the riser when $L = 15$ m, $v = 1$ and $k = 2$ with increasing CF velocities
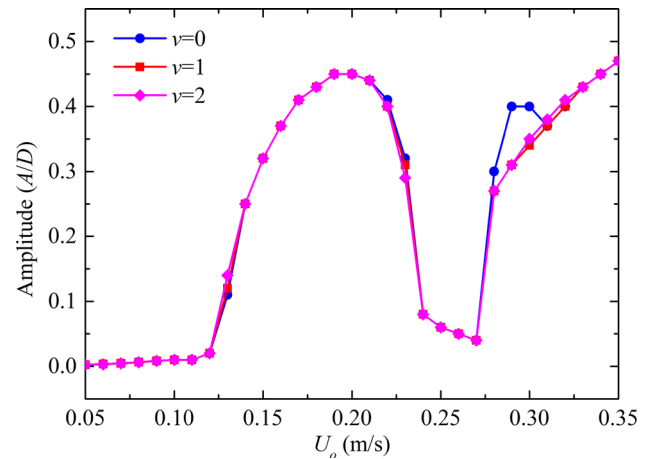
Fig. 5 Displacement amplitudes of the riser for $v = 0$, 1 and 2 with increasing tension coefficient when $L = 150$ m

Table 3 Effect of tension coefficient on the foremost two natural frequencies (rad/s) when $L = 150$ m, $v = 1$

Mode order	Top tension coefficient (k)				
	1	1.5	2	2.5	3
1	0.449	0.672	0.830	0.961	1.075
2	1.073	1.447	1.740	1.989	2.210

Fig. 4 Fundamental frequencies of the riser for $v = 0$, 1 and 2 with increasing tension coefficient when $L = 150$ m

that there are three, two and one lock-in regions of displacement amplitudes when $k = 1$, 2 and 3, respectively. It is also noted that an increase in tension coefficient results in a slightly decrease in displacement amplitude. Moreover, an increase in tension coefficient is accompanied by a right shift in the first lock-in region and a wider synchronization region.

Therefore, in the present model, the tension coefficient $k = 2$ and $v = 1$ is utilized to study the effect of CF velocity on the displacements and stresses, as shown in

Fig. 7. Inspecting Fig. 7, it is found that the displacement amplitudes are in synchronization with the maximum stresses. Moreover, there are two lock-in regions in the range of CF velocities, and the jumping phenomenon is also discovered. Besides, it should be noted that the displacements and stresses are dramatically increased within the renounce regions whereas they are quickly decreased outside the scope of these regions, namely pre-synchronization and post-synchronization regions. This is due to the fact that the lock-in phenomenon results in the displacement and stress amplitude jumping when the vortex-shedding frequency, which is decided by CF velocity for constant structure parameters, is near the natural frequencies of the riser. Therefore, four kinds of CF velocities, namely $U_o = 0.1$, 0.2, 0.25 and 0.35 m/s, are chosen to proceed the research of top harmonic tensions. The range
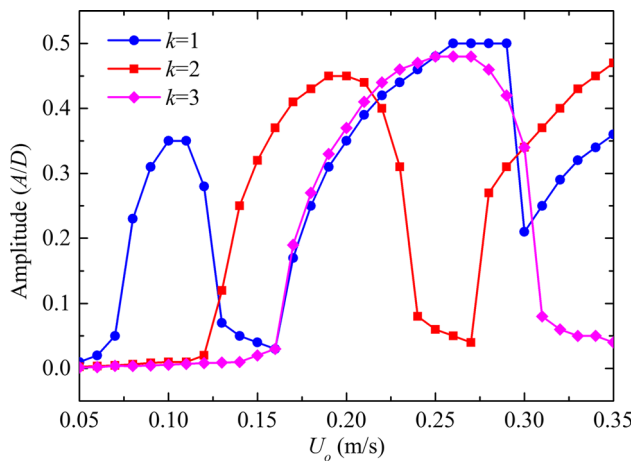
Fig. 6 Maximum displacement amplitudes (A/D) of the flexible riser at $k = 1$, 2 and 3 for $v = 1$ with increasing CF velocity when $L = 150$ m
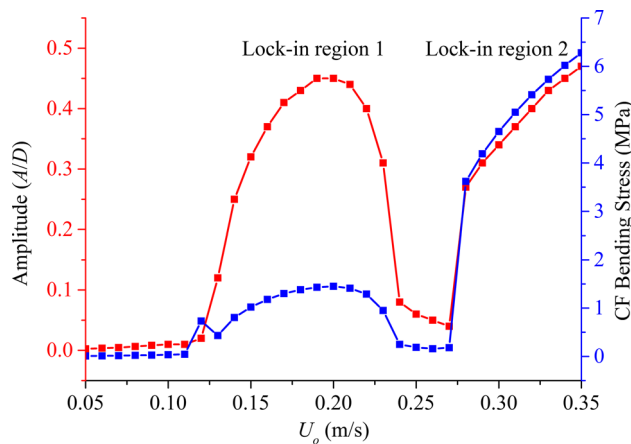
Fig. 7 Displacement amplitudes and Maximum CF bending stresses of the riser when $v = 1$ and $k = 2$ with increasing CF velocities

of excitation frequencies of top tension is within three times values of the fundamental frequency of the riser.

4.3 The dynamic responses of the riser under harmonic tension

The displacement amplitudes as a function of excitation frequency of top pre-tension for varying harmonic tension amplitudes and CF velocities are shown in Fig. 8. It is noted that the CF velocities in Fig. 8a–c are, respectively, located in pre-synchronization, synchronization and post-synchronization regions of the first lock-in region of the CF velocities; the CF velocity of Fig. 8d is within the synchronization region of the second lock-in region.

In Fig. 8a, it is observed that the excitation frequencies have a little effect on the displacement amplitudes of the flexible riser when $a = 0.1$, whereas the displacement amplitude is rapidly changed near twice the fundamental

frequency of the flexible riser when $a = 0.3$ and 0.5. Furthermore, it should be noted that an increase in harmonic tension amplitudes is accompanied by a right shift of the maximum displacement amplitude of the riser in the resonance region and the resonance regions also become wider. Inspecting Fig. 8b, there are two resonance regions which are, respectively, located nearby the fundamental frequency and twice values of the fundamental frequency. Moreover, the excitation frequencies have an important effect on the displacement amplitudes near twice fundamental frequency when $a = 0.1$. A right shift of the lock-in region is also appeared.

However, a left shift of the maximum displacement amplitude of the riser in the resonance region is discovered in Fig. 8c. It is also indicated that the excitation frequencies have a little effect on the displacement amplitudes of the flexible riser when $a = 0.1$; these findings can infer that when the harmonic tension amplitude is low and the CF velocity is out of the range of the lock-in region, the excitation frequency has little effect on the displacement amplitude. Figure 8d shows an intriguing phenomenon that multi-resonance regions emerge, in especially, the lock-in region between the first and second resonance regions.

In general, the results are revealed that the excitation frequencies close to twice values of the fundamental frequency have a significant impact on the displacement amplitudes; this phenomenon confirmed by the experimental research in [31] is a favorable scenario for the principal Mathieu's instability, and the harmonic tension excitation with this frequency does trigger the Mathieu-like resonance [32]. Moreover, it is also revealed that the resonance regions of the excited frequencies are wider with the increase in harmonic tension amplitude due to the fact that an increase in harmonic tension amplitude leads to the wider bandwidth of natural frequency.

Figure 9 presents the effect of excitation frequency on the displacement amplitudes for various harmonic tension amplitudes and CF velocities. Figure 9a–c corresponds to the harmonic tension amplitude $a = 0.1$, 0.3 and 0.5, respectively. The results shown in Fig. 9a illustrate that the large resonance region near twice of the fundamental frequency of the riser occurs in the first lock-in region of CF velocity when $a = 0.1$, whereas a smaller resonance region which is slightly larger than the fundamental frequency appear in the first lock-in region of CF velocity. Besides, the excitation frequencies have little impact on displacement amplitudes when the CF velocities are out of range of the lock-in region.

In Fig. 9b, it is revealed that the resonance regions near twice of fundamental frequency will arise for all of cases and a right shift in the resonance region is observed. Furthermore, the displacement amplitudes are slightly increased when the CF velocities are located in lock-in
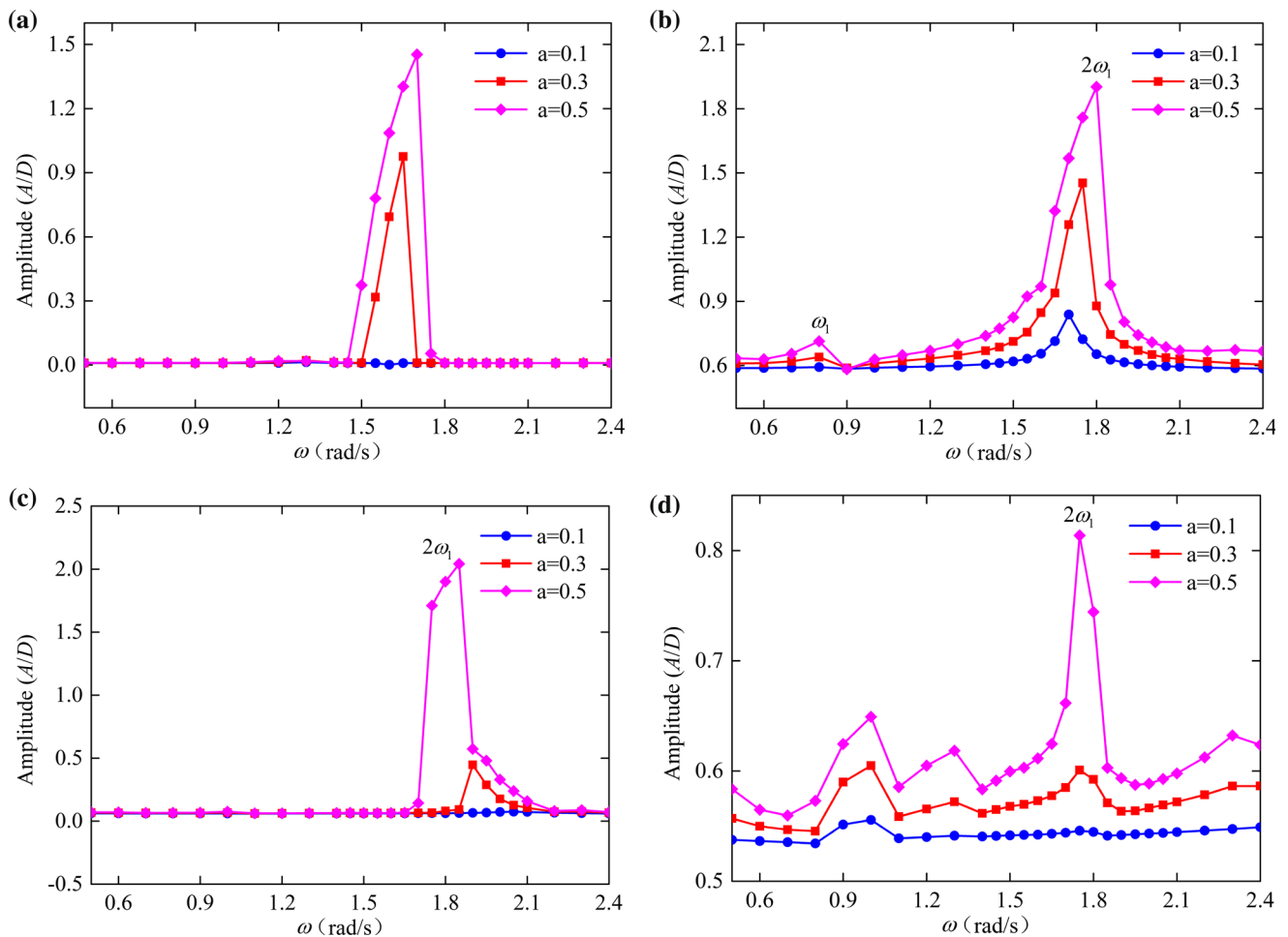
Fig. 8 Displacement amplitudes of the riser for **a** $U_o = 0.1$ m/s, **b** $U_o = 0.2$ m/s, **c** $U_o = 0.25$ m/s and **d** $U_o = 0.35$ m/s with increasing excitation frequencies

regions. However, the displacement amplitudes are dramatically increased with the increase in harmonic tension amplitude and a right shift of resonance region also appeared, as shown in Fig. 9c.

In summary, the smaller harmonic tension amplitude has a slight effect on the displacement amplitude for various CF velocities except $U_o = 0.2$ m/s which is located in the first lock-in region of CF velocities. When the harmonic tension amplitude is increased, the resonances occur for all of CF velocities, but there is a small resonance displacement within the second lock-in CF velocity. Moreover, the shift of resonance frequency region is due to the fact that the stronger sub-harmonic components participate in which is validated in [33]. In addition, vortex-shedding frequency decided by the CF velocity also has a significant effect.

As for the transverse bending stress of the marine riser, it can be calculated by Eq. (8). The positive and negative signs represent compressive and bending stresses in CF direction.

$$\sigma_w(z,t) \approx \pm \frac{D}{2} E w''(z,t) \qquad (8)$$

Figure 10 presents the influences of excitation frequency on the maximum CF bending stresses of the riser for varying harmonic tension amplitudes when $U_o = 0.1$, 0.2, 0.25 and 0.35 m/s. Inspecting Fig. 10a, c, it is found that the maximum stress has the same tendency with the displacement amplitude for all case of analysis conditions. The results also show that the maximum stress is sharply increased within the resonance regions. However, it can be seen from Fig. 10b that there is another resonance region of stresses between the first and second lock-in regions of the displacement amplitudes. It is also revealed that the resonance region is near twice of the fundamental frequency dominating the displacement and stress responses in the case.

Figure 10d portrays the maximum CF bending stress responses for different harmonic tension amplitudes when CF velocity is within the second lock-in region (see Fig. 7).
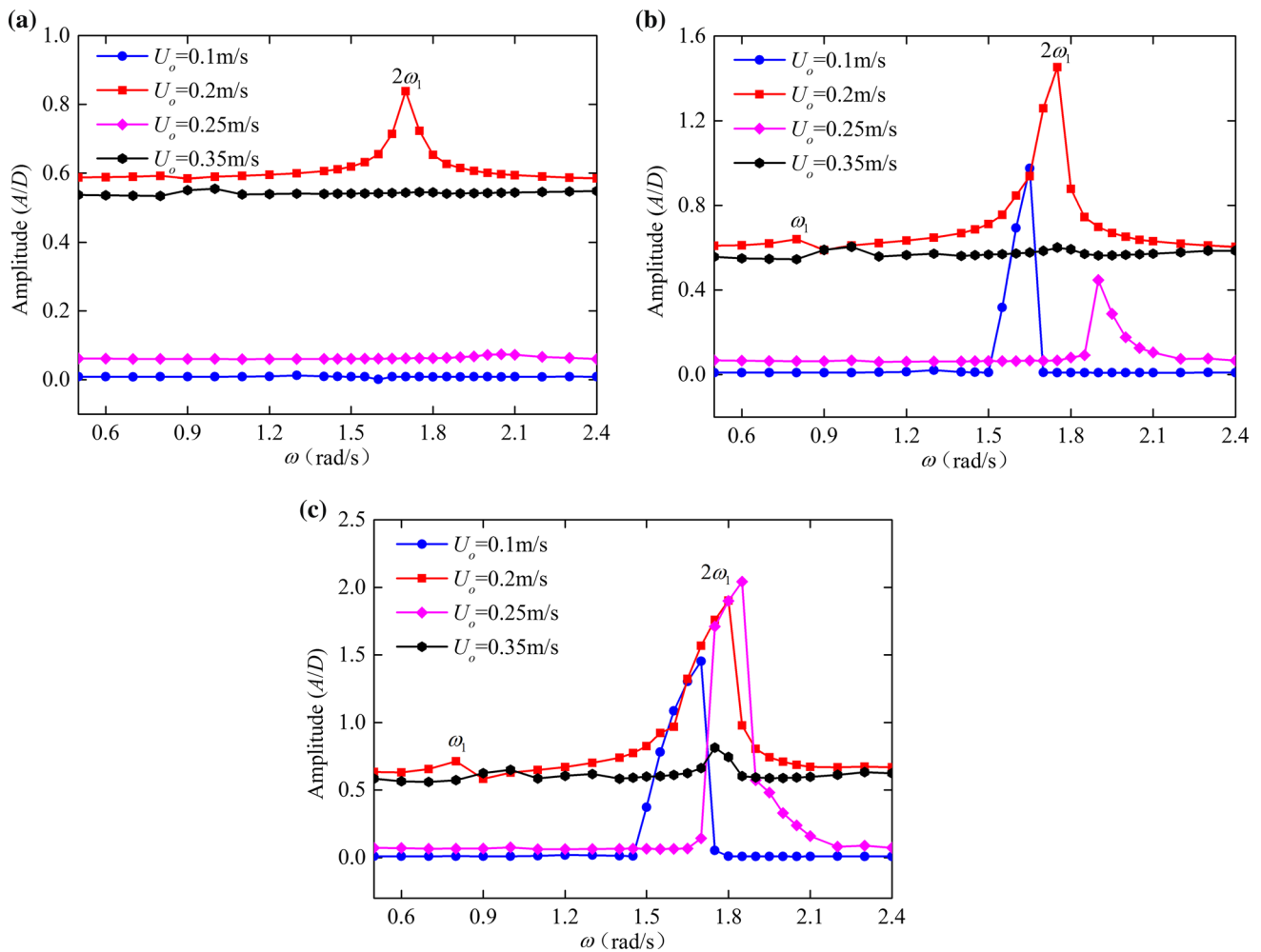
Fig. 9 Displacement amplitudes of the riser for **a** $a = 0.1$, **b** $a = 0.3$ and **c** $a = 0.5$ with increasing excitation frequencies

Although the resonance region is near twice of the fundamental frequency and dominates the displacement responses (see Fig. 8d), the resonance regions nearby the fundamental frequency play a leading role in the stress responses. Besides, the maximum stresses are first rapidly decreased and then dramatically increased when the harmonic tension amplitudes are enough large. More wide lock-in regions are also observed with the increase in harmonic tension amplitude for all of cases. The reason is that excitation frequencies within the resonance region are close to the second natural frequency of the riser.

It can be obtained from Fig. 10 that the same regularities were observed near the first lock-in region of CF velocities. However, the fundamental frequency dominates the stress responses when CF velocity is within the second lock-in region; this may be because the sub-harmonic components participate in the mode jumps and multi-frequencies response superposition.

The effects of excitation frequency on the maximum CF bending stresses of the riser for varying CF velocities when $a = 0.1$, 0.3 and 0.5 is illustrated in Fig. 11a–c, respectively. The plotted curves in Fig. 11a show that the excitation frequencies have a little impact on the CF bending stresses when CF velocities are located in pre-synchronization and post-synchronization regions. As CF velocity is within the first lock-in region, there are two resonance regions and the second resonance region will dominate the stress responses. Besides, the first resonance has the maximum CF bending stress.

It can be seen from Fig. 11b that an increase in CF velocity results in the increase in stress amplitudes and a right shift of resonance regions near twice fundamental frequency. Moreover, the excitation frequency near the fundamental frequency will dominate the stress responses. For $a = 0.5$, it is found from Fig. 11c that the resonance region near twice fundamental frequency is observed for all cases of CF velocity. A right shift in resonance regions are also observed near the first lock-in region of CF velocity. In general, the excitation frequency near twice fundamental frequency plays an important role in the displacement and
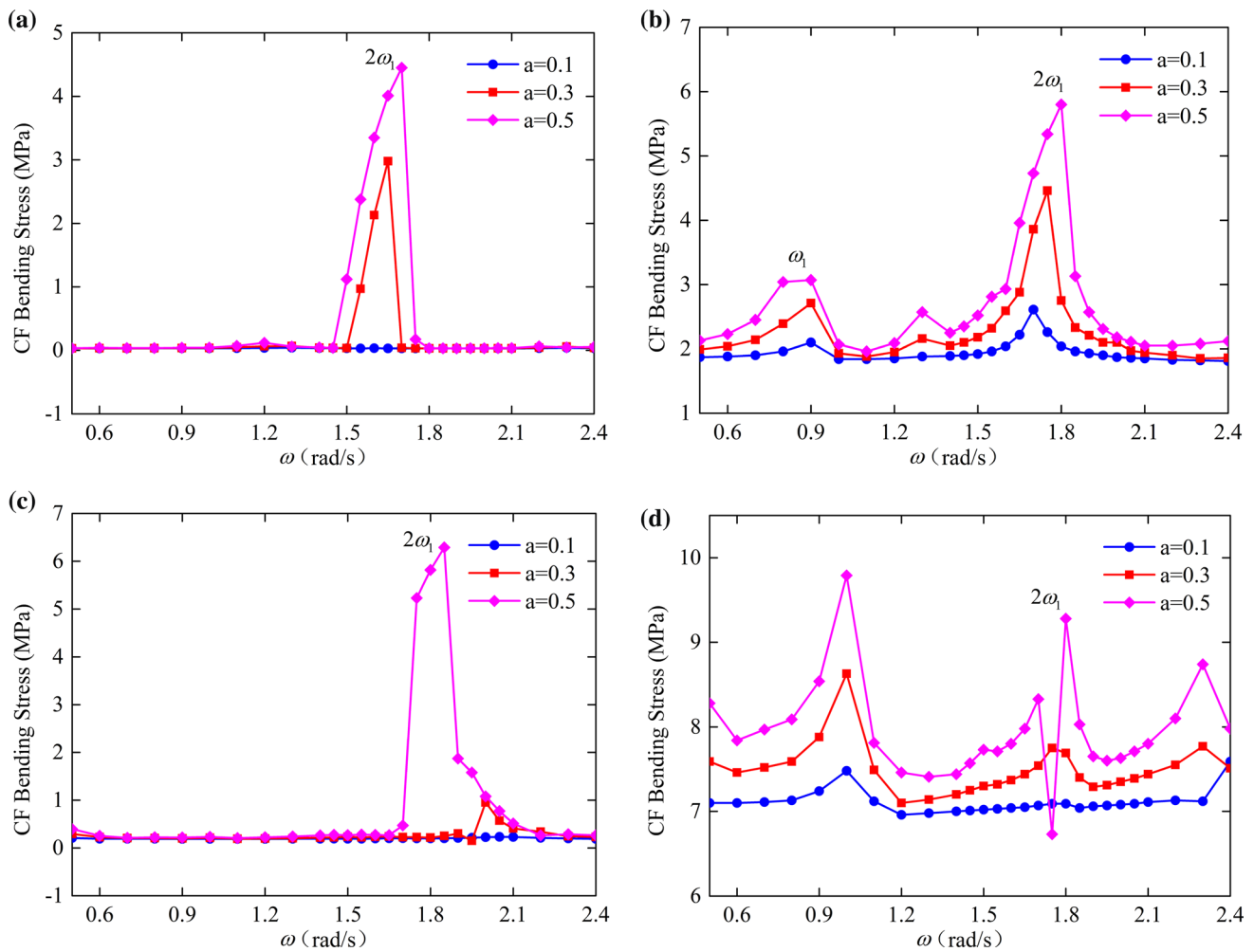
Fig. 10 Maximum CF bending stresses of the riser for **a** $U_o = 0.1$ m/s, **b** $U_o = 0.2$ m/s, **c** $U_o = 0.25$ m/s and **d** $U_o = 0.35$ m/s with increasing excitation frequencies

stress responses for the first lock-in region of CF velocity. It can be also inferred that the excitation frequency near fundamental frequency will dominate the displacement and stress responses beyond the first lock-in region of CF velocity.

It can be found from Fig. 8–11 that vortex-shedding frequency related to both CF velocity and the hormonic tension has an important impact on the displacement and stress resonances. Furthermore, it should be noted that the time-varying harmonic tension will affect the natural frequencies of the riser. In addition, the natural frequencies will influence the lock-in region of CF velocities. This interactive relationship results in the emergence of the aforementioned complex phenomena.

Figure 12 presents the space-time responses of CF displacement corresponding to the displacement amplitudes plotted in Fig. 8b for different harmonic tension coefficients when $\omega = 0.9$ rad/s and $U_o = 0.2$ m/s, namely the first resonance region excited by hormonic tension

frequency. It is found that the displacement responses show beating patterns, and this phenomenon will enhance with the increase in harmonic tension coefficient. Moreover, an increase in harmonic tension coefficient leads to the increase in the maximum displacement amplitude.

Figure 13 portrays the space-time responses of CF displacement corresponding to the displacement amplitudes plotted in Fig. 8b for a = 0.1, 0.3 and 0.5, respectively, corresponding to $\omega = 1.7$ rad/s, $\omega = 1.75$ rad/s and $\omega = 1.8$ rad/s when $U_o = 0.2$ m/s. The results revealed that the displacement responses located in the maximum resonance region keep pace with the excitation frequencies. It is also found that the maximum displacement amplitudes are dramatically increased with increasing the harmonic tension amplitude at these resonance frequencies.
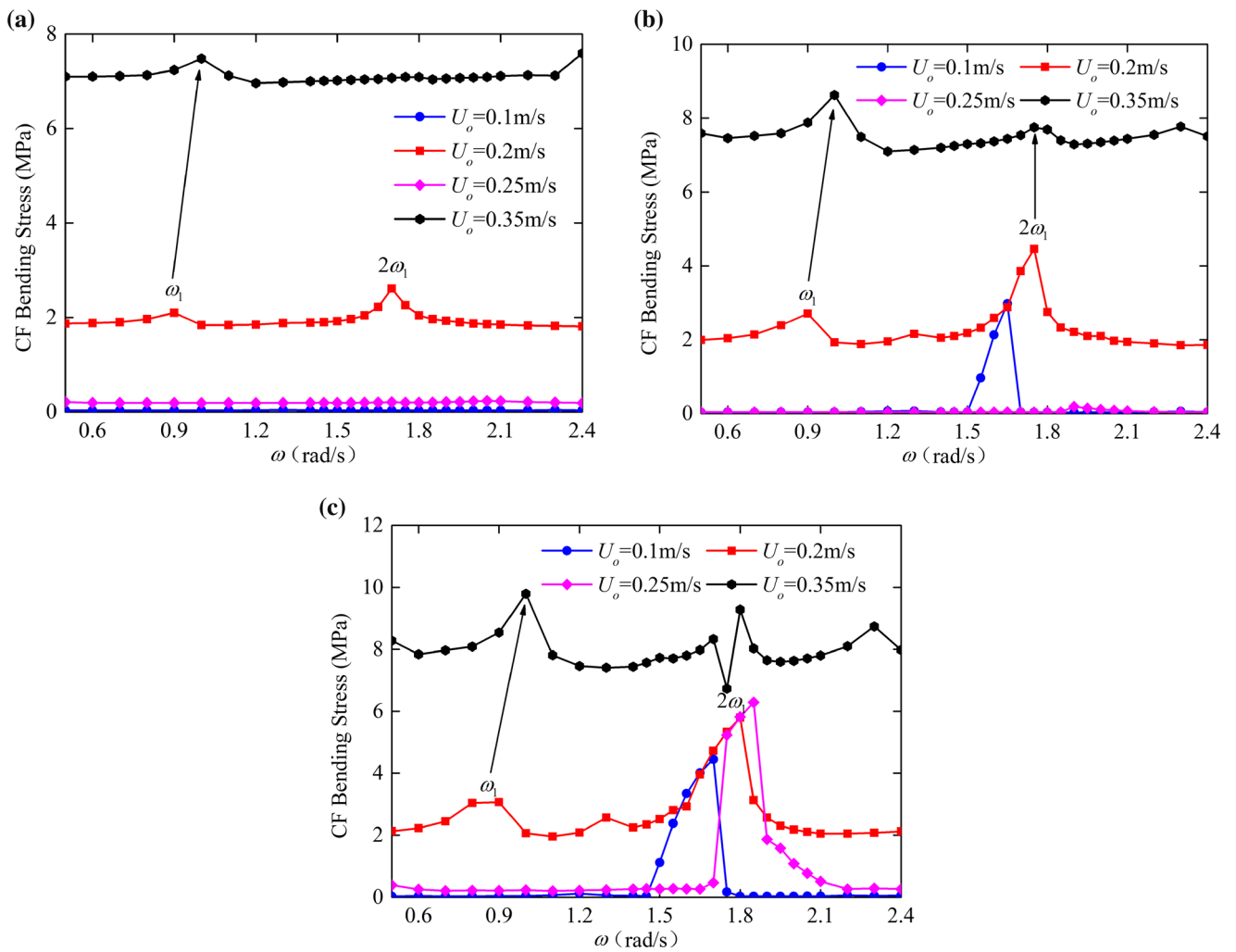
Fig. 11 Maximum CF bending stresses of the riser for **a** $a = 0.1$, **b** $a = 0.3$ and **c** $a = 0.5$ with increasing excitation frequencies
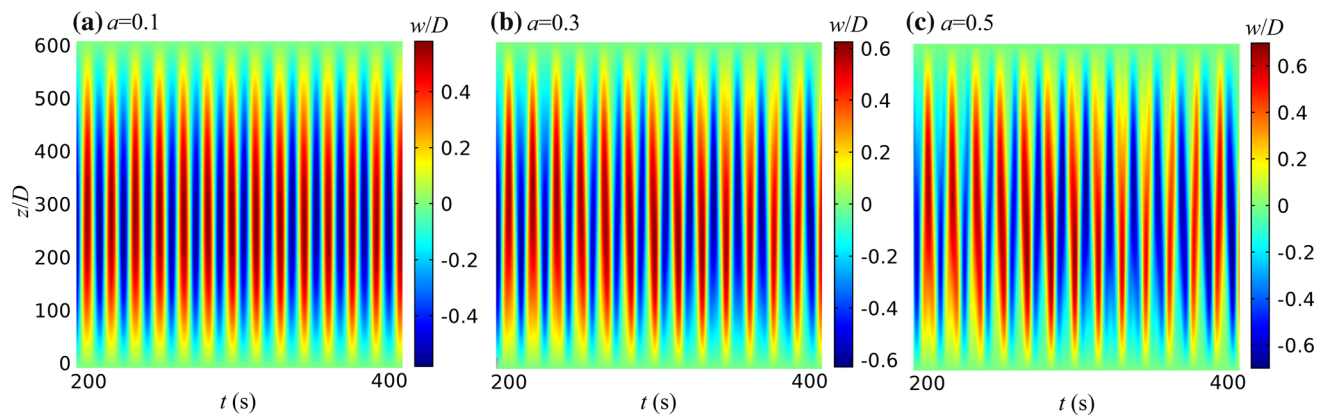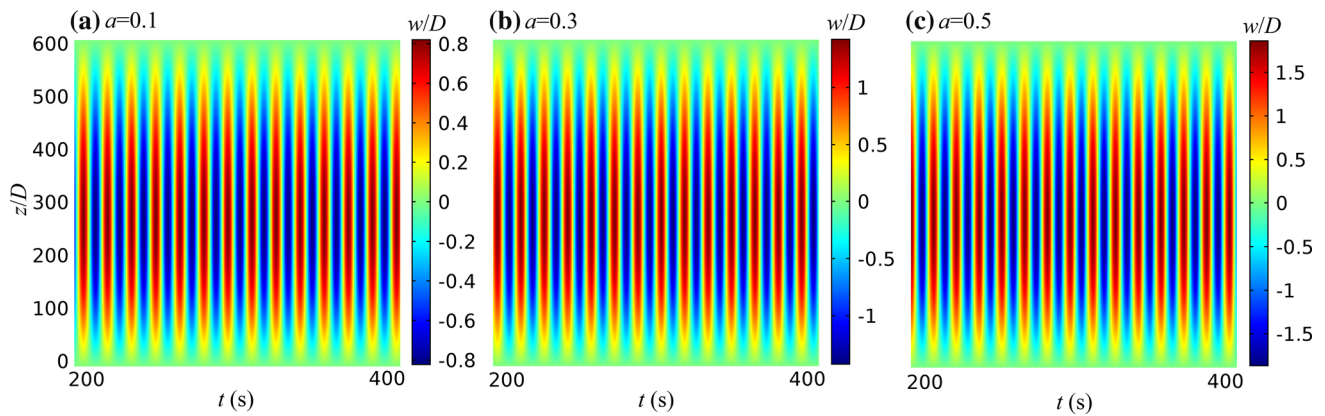

Fig. 12 Space-time-varying responses of CF displacement for $\omega = 0.9$ rad/s when $U_o = 0.2$ m/s

Fig. 13 Space-time-varying responses of CF displacement for **a** $\omega = 1.7$ rad/s, **b** $\omega = 1.75$ rad/s and **c** $\omega = 1.8$ rad/s when $U_o = 0.2$ m/s

5 Conclusions

In the present work, a CF VIV dynamic model of a marine riser transporting fluid subjected to top harmonic tension was investigated by FEM. The nonlinear hydrodynamic force that is expressed as the component sum of drag and lift along the CF direction was also introduced in the present model. A wake oscillator model was used to represent the CF excitation. It was found that the internal fluid velocity has little influence on fundamental frequency and displacement amplitude for our model in this paper.

For constant top tension, the frequency analyses demonstrated that an increase in the top tension leads to the increase in natural frequency of the riser. The two lock-in regions were also observed in the range of analysis parameters. It should be noted that the displacement amplitudes and stresses are dramatically increased in the lock-in regions.

As for top harmonic tension, the excitation frequency near twice fundamental frequency plays an important role in the displacement and stress responses within the first lock-in region of CF velocity whereas the excitation frequency near the fundamental frequency dominates when CF velocity is far away from the first lock-in region and harmonic tension amplitude is larger. It should be noted that an increase in harmonic tension amplitude results in the increase in displacements and stresses. In addition, the resonance regions become wider and the first resonance regions of excitation frequency also appeared. Moreover, it was also demonstrated that the maximum displacement amplitudes of the riser show a right shift within pre-synchronization and synchronization whereas a left shift is observed in post-synchronization.

The space-time-varying responses showed that the beating patterns are produced near the first resonance region of excitation frequencies. As for the second resonance region of excitation frequencies, the displacement responses locate in the maximum resonance region keep pace with the excitation frequencies. A model, including the IL and AX motions, should be investigated to reveal the new intriguing dynamic phenomenon in the future. Besides, the present work can guide the usage of marine riser and suppress the VIV by applying appropriate harmonic tension for various CF velocities. In the future, some intriguing fluid-structure interaction phenomena need to be explored by combined both IL and CF top excitations.

References

1. Wang J, Fu S, Baarholm R, Wu J, Larsen CM (2014) Fatigue damage of a steel catenary riser from vortex-induced vibration caused by vessel motions. Mar Struct 39(39):131–156
2. Wang KP, Xue HX, Tang WY (2013) In-Line VIV response and fatigue damage of a deepwater riser in linearly sheared flow. J Vib Shock 32(19):1–6
3. Xue H, Tang W, Qu X (2014) Prediction and analysis of fatigue damage due to cross-flow and in-line VIV for marine risers in non-uniform current. Ocean Eng 83(2):52–62
4. Brika D, Laneville A (2006) Vortex-induced vibrations of a long flexible circular cylinder. J Fluid Mech 250(250):481–508
5. Wang E, Xiao Q (2016) Numerical simulation of vortex-induced vibration of a vertical riser in uniform and linearly sheared currents. Ocean Eng 121:492–515
6. Bahmani MH, Akbari MH (2011) Response characteristics of a vortex-excited circular cylinder in laminar flow. J Mech Sci Technol 25(1):125–133. https://doi.org/10.1007/s12206-010-1021-0
7. Huera-Huarte FJ, Bearman PW (2009) Wake structures and vortex-induced vibrations of a long flexible cylinder—part 1: dynamic response. J Fluids Struct 25(6):969–990
8. Bearman PW (2011) Circular cylinder wakes and vortex-induced vibrations. J Fluids Struct 27(5–6):648–658
9. Gabbai RD, Benaroya H (2005) An overview of modeling and experiments of vortex-induced vibration of circular cylinders. J Sound Vib 282(3–5):575–616

10. Sarpkaya T (2004) A critical review of the intrinsic nature of vortex-induced vibrations. J Fluids Struct 19(4):389–447
11. Williamson CHK, Govardhan R (2004) Vortex-induced vibrations. Annu Rev Fluid Mech 36(1):413–455
12. Wu X, Ge F, Hong Y (2012) A review of recent studies on vortex-induced vibrations of long slender cylinders. J Fluids Struct 28(1):292–308
13. Facchinetti ML, de Langre E, Biolley F (2004) Coupling of structure and wake oscillators in vortex-induced vibrations. J Fluids Struct 19(2):123–140. https://doi.org/10.1016/j.jfluidstructs.2003.12.004
14. Srinil N, Zanganeh H (2012) Modelling of coupled cross-flow/in-line vortex-induced vibrations using double Duffing and van der Pol oscillators. Ocean Eng 53:83–97. https://doi.org/10.1016/j.oceaneng.2012.06.025
15. Zanganeh H, Srinil N (2014) Characterization of variable hydrodynamic coefficients and maximum responses in two-dimensional vortex-induced vibrations with dual resonances. J Vib Acoust 136(5):051014
16. Postnikov A, Pavlovskaia E, Wiercigroch M (2017) 2DOF CFD calibrated wake oscillator model to investigate vortex-induced vibrations. Int J Mech Sci 127:176–190. https://doi.org/10.1016/j.ijmecsci.2016.05.019
17. Srinil N (2011) Analysis and prediction of vortex-induced vibrations of variable-tension vertical risers in linearly sheared currents. Appl Ocean Res 33(1):41–53. https://doi.org/10.1016/j.apor.2010.11.004
18. Dai HL, Abdelkefi A, Wang L (2014) Modeling and nonlinear dynamics of fluid-conveying risers under hybrid excitations. Int J Eng Sci. https://doi.org/10.1016/j.ijengsci.2014.03.009
19. Dai HL, Wang L, Qian Q, Ni Q (2013) Vortex-induced vibrations of pipes conveying fluid in the subcritical and supercritical regimes. J Fluids Struct 39:322–334. https://doi.org/10.1016/j.jfluidstructs.2013.02.015
20. Dai HL, Wang L, Qian Q, Ni Q (2014) Vortex-induced vibrations of pipes conveying pulsating fluid. Ocean Eng 77:12–22. https://doi.org/10.1016/j.oceaneng.2013.12.006
21. He F, Dai H, Huang Z, Wang L (2017) Nonlinear dynamics of a fluid-conveying pipe under the combined action of cross-flow and top-end excitations. Appl Ocean Res 62:199–209. https://doi.org/10.1016/j.apor.2016.12.007
22. Meng SH, Zhang XQ, Che CD, Zhang WJ (2017) Cross-flow vortex-induced vibration of a flexible riser transporting an internal flow from subcritical to supercritical. Ocean Eng 139:74–84. https://doi.org/10.1016/j.oceaneng.2017.04.039
23. Yuan YC, Xue HX, Tang WY (2017) An improved time domain coupled model of cross-flow and in-line vortex-induced vibration for flexible risers. Ocean Eng 136:117–128. https://doi.org/10.1016/j.oceaneng.2017.03.018
24. Srinil N (2010) Multi-mode interactions in vortex-induced vibrations of flexible curved/straight structures with geometric nonlinearities. J Fluids Struct 26(7–8):1098–1122. https://doi.org/10.1016/j.jfluidstructs.2010.08.005
25. Srinil N, Wiercigroch M, O'Brien P (2009) Reduced-order modelling of vortex-induced vibration of catenary riser. Ocean Eng 36(17–18):1404–1414. https://doi.org/10.1016/j.oceaneng.2009.08.010
26. Zanganeh H, Srinil N (2016) Three-dimensional VIV prediction model for a long flexible cylinder with axial dynamics and mean drag magnifications. J Fluids Struct 66:127–146. https://doi.org/10.1016/j.jfluidstructs.2016.07.004
27. Song J-n LuL, Teng B, H-i Park, Tang G-q WuH (2011) Laboratory tests of vortex-induced vibrations of a long flexible riser pipe subjected to uniform flow. Ocean Eng 38(11–12):1308–1322. https://doi.org/10.1016/j.oceaneng.2011.05.020
28. Yang W, Ai Z, Zhang X, Gou R, Chang X (2018) Nonlinear three-dimensional dynamics of a marine viscoelastic riser subjected to uniform flow. Ocean Eng 149:38–52. https://doi.org/10.1016/j.oceaneng.2017.12.004
29. Yang W, Ai Z, Zhang X, Chang X, Gou R (2018) Nonlinear dynamics of three-dimensional vortex-induced vibration prediction model for a flexible fluid-conveying pipe. Int J Mech Sci 138–139:99–109. https://doi.org/10.1016/j.ijmecsci.2018.02.005
30. Sanaati B, Kato N (2012) A study on the effects of axial stiffness and pre-tension on VIV dynamics of a flexible cylinder in uniform cross-flow. Appl Ocean Res 37:198–210. https://doi.org/10.1016/j.apor.2012.05.001
31. Franzini GR, Pesce CP, Salles R, Gonçalves RT, Fujarra ALC, Mendes P (2014) Experimental analysis of a vertical and flexible cylinder in water: response to top motion excitation and parametric resonance. J Vib Acoust 137(3):031010
32. Franzini GR, Santos CCP, Mazzilli CEN, Pesce CP (2016) Parametric excitation of an immersed, vertical and slender beam using reduced-order models: influence of hydrodynamic coefficients. Mar Syst Ocean Technol 11(1):1–9
33. Yuan Y, Xue H, Tang W (2018) A numerical investigation of Vortex-Induced Vibration response characteristics for long flexible cylinders with time-varying axial tension. J Fluids Struct 77:36–57. https://doi.org/10.1016/j.jfluidstructs.2017.12.004